


## RESEARCH ARTICLE

# Regional oligodendrocytopathy and astrocytopathy precede myelin loss and blood–brain barrier disruption in a murine model of osmotic demyelination syndrome

Joanna Bouchat<sup>1</sup> | Bruno Couturier<sup>2,3</sup> | Catherine Marneffe<sup>1</sup> |  
 Fabrice Gankam-Kengne<sup>3,4</sup> | Benoît Balau<sup>1</sup> | Kathleen De Swert<sup>1</sup> |  
 Jean-Pierre Brion<sup>3</sup> | Luc Poncelet<sup>5</sup> | Jacques Gilloteaux<sup>1,6</sup> | Charles Nicaise<sup>1</sup> 

<sup>1</sup>URPhyM – NARILIS, Université de Namur, Namur, Belgium

<sup>2</sup>Department of General Medicine, Erasme Hospital, Université Libre de Bruxelles, Bruxelles, Belgium

<sup>3</sup>Laboratory of Histology, Neuroanatomy and Neuropathology, Université Libre de Bruxelles, Bruxelles, Belgium

<sup>4</sup>Department of Nephrology, EpiCURA Ath, Ath, Belgium

<sup>5</sup>Laboratory of Anatomy, Biomechanics and Organogenesis, Université Libre de Bruxelles, Bruxelles, Belgium

<sup>6</sup>Department of Anatomical Sciences, St George's University School of Medicine, Newcastle upon Tyne, United Kingdom

## Correspondence

Charles Nicaise, URPhyM – NARILIS, Université de Namur, Faculté de Médecine, Rue de Bruxelles 61, 5000 Namur, Belgium.  
 Email: charles.nicaise@unamur.be

## Abstract

The osmotic demyelination syndrome (ODS) is a non-primary inflammatory disorder of the central nervous system myelin that is often associated with a precipitous rise of serum sodium concentration. To investigate the physiopathology of ODS *in vivo*, we generated a novel murine model based on the abrupt correction of chronic hyponatremia. Accordingly, ODS mice developed impairments in brainstem auditory evoked potentials and in grip strength. At 24 hr post-correction, oligodendrocyte markers (APC and Cx47) were downregulated, prior to any detectable demyelination. Oligodendrocytopathy was temporally and spatially correlated with the loss of astrocyte markers (ALDH1L1 and Cx43), and both with the brain areas that will develop demyelination. Oligodendrocytopathy and astrocytopathy were confirmed at the ultrastructural level and culminated with necroptotic cell death, as demonstrated by pMLKL immunoreactivity. At 48 hr post-correction, ODS brains contained pathognomonic demyelinating lesions in the pons, mesencephalon, thalamus and cortical regions. These damages were accompanied by blood–brain barrier (BBB) leakages. Expression levels of IL-1 $\beta$ , FasL, TNFRSF6 and LIF factors were significantly upregulated in the ODS lesions. Quiescent microglial cells type A acquired an activated type B morphology within 24 hr post-correction, and reached type D at 48 hr. In conclusion, this murine model of ODS reproduces the CNS demyelination observed in human pathology and indicates ambiguous causes that is regional vulnerability of oligodendrocytes and astrocytes, while it discards BBB disruption as a primary cause of demyelination. This study also raises new queries about the glial heterogeneity in susceptible brain regions as well as about the early microglial activation associated with ODS.

## KEYWORDS

astrocyte, blood–brain barrier, mice, microglia, oligodendrocyte, osmotic demyelination syndrome

## 1 | INTRODUCTION

Osmotic demyelination syndrome (ODS) is a non-primary inflammatory disorder of the central nervous system encompassing central pontine

**Abbreviations:**  $\Delta$ Na<sup>+</sup>, gradient of serum Na<sup>+</sup>; BAEP, brainstem auditory evoked potential; BBB, blood–brain barrier; CPM, central pontine myelinolysis; Cx, connexin; DAMP, damage-associated molecular pattern; EPM, extrapontine myelinolysis; ODS, osmotic demyelination syndrome; TEM, transmission electron microscopy.

myelinolysis (CPM) and extrapontine myelinolysis (EPM). This neurological syndrome was first described as a complication of alcoholism and malnutrition (Adams, Victor, & Mancall, 1959). In this condition, patients developed symmetrical demyelinating lesions in centropontine regions, and symptoms such as altered state of consciousness, quadriplegia, pseudobulbar palsy, respiratory insufficiency. In 1976, Tomlinson was the first to establish an association between CPM and electrolyte disturbance (Tomlinson, Pierides, & Bradley, 1976). Few years later, a link between ODS and overly rapid correction of chronic

severe hyponatremia was experimentally confirmed using a rat model (Kleinschmidt-DeMasters & Norenberg, 1981) and by systematic blood analysis of symptomatic ODS patients. Nowadays, plasma sodium level is tightly monitored in patients presenting severe hyponatremia upon hospital admission and clinical guidelines have been issued regarding the management of hyponatremia or its correction to prevent potential, ensuing brain damages (Spasovski et al., 2014). The initial mechanism triggering demyelination remains unclear, although it was suggested that blood-borne myelinotoxic factors or inability of glial cells to restore their stocks of organic osmolytes (lost during chronic hyponatremia) at the time of correction might be responsible for osmotic cell damages (Lien, 1995; Lien, Shapiro, & Chan, 1991). Animal models (i.e., rat and dog) have been generated in order to unravel the selective loss of myelin or oligodendrocytes (Illowsky & Laureno, 1987; Laureno, 1983; Verbalis & Druitarosky, 1988). For instance, the rapid correction of chronic hyponatremia in rats recapitulates human ODS histopathology, including myelin and oligodendrocyte loss with neurons and axons sparing in specific brain regions such as cortical regions, hippocampus and basal ganglia (Gankam Kengne et al., 2011; Kleinschmidt-DeMasters & Norenberg, 1981). In a rat model of ODS, it was previously shown that astrocytes underwent apoptosis before any evidence of myelin or oligodendrocyte loss (Gankam Kengne et al., 2011). Abnormal loss of astrocytic aquaporins has also been demonstrated in human CPM autopsy cases, stressing the involvement of non-oligodendroglial cells in the development of ODS (Popescu et al., 2013). During the course of ODS, microglial cells acquire an activated phenotype and colocalized with the demyelinating lesions, as observed in human cases (Adams et al., 1959; DeLuca, Nagy, Esiri, & Davey, 2002; Popescu et al., 2013) and in the rat model (Gankam-Kengne, Soupart, Pochet, Brion, & Decaux, 2010; Takefuji et al., 2007). The detection of activated microglial cells in ODS lesions has been linked to the secretion of pro-inflammatory cytokines and the clearance of myelin debris or damaged nervous cells (Iwama et al., 2011).

Rats have traditionally been the preferred species used through the ODS research community. Nevertheless, the development of genetically modified animals, which are primarily mouse models, have paved the way for the manipulation of genes or cells possibly relevant to the pathophysiology of ODS. So far, three studies sought to create murine models of ODS (Sugimura et al., 2002; Thurston & Hauhart, 1987; Thurston, Hauhart, & Nelson, 1987). Although the authors noticed neurological symptoms related to ODS, the publications failed to depict the full histopathological outcomes (i.e., myelin loss), or did not temporally investigate the cellular changes that could be observed after correction of hyponatremia.

The present study describes a novel mouse ODS model which reproduces pathologic changes similar to human ODS in specific CNS regions. The CNS changes studied mainly encompass functional and histopathological alterations in the thalamus region and include analysis of molecular and cellular markers along with some preliminary ultrastructural data. Altogether, the study attempts to further clarify the timely progress of the damages pertaining to the oligodendrocytes, astrocytes and microgliaocytes as well as of myelin and blood-brain barrier (BBB) integrity.

## 2 | MATERIALS AND METHODS

### 2.1 | Animals

The experimental protocol was conducted in compliance with the European Communities Council Directives for Animal Experiment (2010/63/EU, 86/609/EEC and 87-848/EEC) and was approved by the Animal Ethics Committee of University of Namur (ethic project n°14-210). Male C57bl/6J mice, aged from 3 to 4 months were included in the study. Unless otherwise specified, any procedure involving anesthesia was performed using i.p. injection of a cocktail of Ketamine 100 mg/kg and Xylazine 5 mg/kg.

### 2.2 | ODS protocol

ODS induction was based on the correction of a chronic dilutional hyponatremia, according to an adapted protocol (Verbalis & Druitarosky, 1988). Briefly, an osmotic minipump (Model 1004, Alzet, Cupertino, CA) was filled with desmopressin acetate (0.002 mg/ml; Minirin, Ferring, Saint-Prex, Switzerland) and inserted subcutaneously under anesthesia into the back of animals at day 0. Standard pellets and water were switched to a low-sodium liquid diet (AIN76A, MP Biomedicals, Santa Ana, CA), given *ad libitum* for the whole duration of hyponatremia. At day 4, hyponatremia level was measured and serum sodium was increased close to normonatremia using a single intraperitoneal injection of NaCl 1M (1.5 ml/100 g body weight). Minipumps were left into animals until the end of experiments. Animals had access to standard pellets and water *ad libitum* at day 5, after natremia measurement. All animals were daily monitored according to a previously described neurological scale (Sugimura et al., 2005).

### 2.3 | Natremia measurements

After topical application of lidocaine, blood samples (25  $\mu$ l) were collected by tail puncture. Natremia was measured on whole-blood sample on Spotchem EL SE-1520 electrolyte analyzer (Arkay, Kyoto, Japan) using ion-selective electrodes and potentiometry. Some samples were compared with standard flame spectrophotometry (Supporting Information, Figure S1).

### 2.4 | Grip strength

Limb muscle strength was determined using a Grip Strength Meter (Bioseb, Vitrolles, France). Grip strength testing was performed by allowing the animals to grasp a grid attached to the force gauge using all four limbs. This was followed by pulling the animal away from the gauge until the limbs released the grid, this provides a value for the force of maximal grip strength. The force measurements were recorded in three trials, and the averages were used in analyses.

### 2.5 | Brainstem auditory evoked potentials

Mice were anesthetized using isoflurane (1.5%) in oxygen inhalation. They were placed on a heating pad and their body temperature was maintained throughout the experiment. Adapted insets were connected

**TABLE 1** Antibodies used in immunohistochemistry

Antigen	Supplier – reference	Dilution
ALDH1L1	Abcam – ab87117	1:1000
APC (clone CC1)	Calbiochem – OP80	1:50
AQP4	Merck – AB3594	1:1000
Cx43	Abcam – ab11370	1:1000
Cx47	Life Technologies – 374500	1:200
GFAP	Sigma-Aldrich – G3893	1:1000
Iba1	Wako – 019-19741	1:1000
MBP	Abcam – ab40390	1:500
pMLKL	Abcam – ab196436	1:1000
Olig2	Merck – MABN50	1:100
SMI94	Eurogentec – SMI-94R	1:100
S100 $\beta$	Dako – Z0311	1:100

to earphones (Caldwell 10 Ohms) by 10 cm silicone tubing and were inserted into both ear canals. The left ear was stimulated using clicks of 0.1 ms duration and 90 dB normal hearing level intensity delivered at 11.1/s, while the right ear received a continuous 60 dB masking noise from the stimulator (Caldwell Sierra II XP). Brainstem auditory evoked potentials (BAEPs) were recorded using subdermal needle electrodes: the electrode connected to the non-inverting input of the preamplifier was positioned at the vertex of the skull and the one connected to the inverting input was inserted at the level of the left mastoid process; the ground electrode was inserted at the neck level. The amplitude and latency of peaks I–V were measured using the Caldwell Wedge 3.3.3. software.

## 2.6 | Histology and immunohistochemistry

Under anesthesia, mice were exsanguinated and transcardially perfused with NaCl 0.9% followed by phosphate-buffered 4% paraformaldehyde (PFA). Brains were removed, divided into two hemispheres and post-fixed overnight in fixative. Brains were then dehydrated, paraffin-embedded and processed into 6- $\mu$ m sections using a microtome. Paraffin sections were dewaxed, rehydrated and stained with Eriochrome Cyanine R/Cresyl Violet or Perls Prussian blue according to previously published protocols (Nicaise et al., 2009; Nicaise et al., 2012). Sections were dehydrated in ethanol 95% and mounted in DPX (Merck Millipore, Darmstadt, Germany).

For immunohistochemistry, sections were dewaxed, rehydrated and heat-induced antigen retrieval was performed in citrate buffer pH 6 at 100°C for 10 min. Endogenous peroxidase was quenched using 3% H<sub>2</sub>O<sub>2</sub> in methanol for 10 min. Non-specific binding was blocked using 5% horse or goat serum diluted in Tris-buffered saline (TBS) for 15 min. Primary antibodies (Table 1) were diluted into TBS and sections were incubated overnight at 4°C. Next, sections were incubated with a biotinylated secondary antibody (1:100, Vectastain, Vector Laboratories, Burlingame, CA) for 1 hr at room temperature. Sections were then

incubated with a solution of peroxidase-bound streptavidin (1:100; Vectastain) for 45 min. Revelation was done using diaminobenzidine substrate (Dako, Glostrup, Denmark). Finally, sections were counterstained with hemalum, dehydrated and mounted in DPX. For double immunofluorescences, fluorescent secondary antibodies were used at a concentration of 1:100 (Life Technologies, anti-mouse A11001 and A11004, anti-rabbit A11008 and A11011). We used a mounting medium containing DAPI (Life Technologies, Bleiswijk, Netherlands). Detection of apoptosis was performed using Apoptag Fluorescein In Situ Apoptosis Detection Kit according to manufacturer's instructions (Merck Millipore, Overijse, Belgium). Sections were observed with an Olympus BX63 microscope (Olympus, Tokyo, Japan) equipped with Hamamatsu Orca-ER camera and images were acquired with the Cell Sens software.

## 2.7 | Image quantification

Measurements within images were carried out after import in open-access ImageJ software (<https://imagej.nih.gov/ij/>). The quantitative evaluation of stainings was blindly performed by three investigators (C. N., C. M., and J. B.): areas of immunoreactivity were delimited freehand and normalized to total prosencephalon or thalamic nuclei. The number of immunoreactive cells was normalized to thalamus area. The morphology of Iba1<sup>+</sup> microglial cells was analyzed according to Sanchez-Guajardo and others (Sanchez-Guajardo, Febbraro, Kirik, & Romero-Ramos, 2010). Three random pictures were taken using a 40 $\times$  magnification in the thalamus, where Iba1<sup>+</sup> cells were counted and classified into four types based on their morphology. Type A resting: cells have long and very thin processes; Type B ramified: processes are long and dense, cytoplasm around nucleus is visible; Type C ramified: processes are shorter and there are many branches; Type D amoeboid: there is no more processes, the cell is limited to nucleus and strong immunoreactive cytoplasm.

## 2.8 | Ultrastructural observations

Under anesthesia, mice were exsanguinated and transcardially perfused with a solution of PFA 2% and glutaraldehyde 2% in 0.1 M phosphate buffer (pH 7.4). Selected brain regions were harvested and post-fixed in glutaraldehyde 4% for 2 hr. Tissues were washed in Millonig's buffer containing 0.5% sucrose for 24 hr and were then post-fixed in OsO<sub>4</sub> 2%, dehydrated and finally embedded in epoxy resin. Semi-thin sections were stained with toluidine blue. Ultrathin sections were cut with a diamond blade on an ultramicrotome and collected on 300 mesh nickel grids. Thereafter samples were stained with lead citrate and uranyl acetate and observed using a Philips Tecnaï 10 electron microscope.

## 2.9 | RNA isolation and qRT-PCR

Under anesthesia, mice were exsanguinated and transcardially perfused with cold NaCl 0.9%. Brains were harvested, thalamus were micro-dissected, snap-frozen in liquid nitrogen and then stored at –80°C. Thawed samples were homogenized in Trizol reagent (Life



TABLE 2 List of primers

Gene accession number	Sequence	Amplicon size (bp)
BDNF NM_007540.4	Sense 5'-GCAGGTTTCGAGAGGTCTGAC-3'	138
	Antisense 5'-CACCCGGGAAGTGTACAAGT-3'	
CNP1 NM_001146318.1	Sense 5'-CGA-GTG-CAA-GAC-GCT-ATT-CA-3'	121
	Antisense 5'-CTT-GTA-AGC-ATC-AGC-GGA-CA-3'	
Cx43 NM_010288.3	Sense 5'-GGACTGCTTCCTCTCACGTC-3'	126
	Antisense 5'-TCCTTAACGCCCTTGAAGAA-3'	
Cx47 NM_080454.4	Sense 5'-GCATCCAGAGGGAGGCCTGAT-3'	180
	Antisense 5'-CGGTTGGCCGCGACACGAA-3'	
FasL NM_010177.4	Sense 5'-AAGGTGGCCTTGTGATCAAC-3'	84
	Antisense 5'-GCTGGTTGTTGCAAGACTGA-3'	
GDNF NM_010275.3	Sense 5'-CAGCCCAGAGAATTCCAGAG-3'	111
	Antisense 5'-CATAGCCCAAACCCAAGTC-3'	
IL-1 $\beta$ NM_008361.4	Sense 5'-CCCAAGCAATACCCAAAGAA-3'	133
	Antisense 5'-GCTTGTGCTCTGCTTGTGAG-3'	
iNOS NM_010927.4	Sense 5'-TGGTGGTGACAAGCACATTT-3'	119
	Antisense 5'-AAGGCCAAACACAGCATACC-3'	
LIF NM_008501.2	Sense 5'-GTCTGTGCAACAAGTACCGTGT-3'	137
	Antisense 5'-GACCACCACACTTATGACTTGC-3'	
PLP1 NM_011123.3	Sense 5'-AGG-ACA-TCC-CGA-CAA-GTT-TG-3'	120
	Antisense 5'-GAC-TGA-CAG-GTG-GTC-CAG-GT-3'	
TNFRSF6 NM_007987.2	Sense 5'-TGCTTGCTGGCTCACAGTTA-3'	133
	Antisense 5'-CAAATGGCCTCCTTGATA-3'	
TNF- $\alpha$ NM_013693.3	Sense 5'-ACGGCATGGATCTCAAAGAC-3'	116
	Antisense 5'-GTGGGTGAGGAGCACGTAGT-3'	
HPRT NM_013556.2	Sense 5'-GGACCTCTCGAAGTGTGGAT-3'	70
	Antisense 5'-CCAACAACAACTTGTCTGGAA-3'	

Technologies, Bleiswijk, The Netherlands) and total RNA was further isolated according to manufacturer's instructions including a step of purification using the High Pure RNA Tissue Kit (Roche Diagnostics, Basel, Switzerland). RNA concentrations were measured using a spectrophotometer Nanodrop 1000 (Thermo Scientific, Bleiswijk, The Netherlands). Total RNA was reverse-transcribed using the Super Script II RNase H reverse transcriptase kit (Invitrogen, Merelbeke, Belgium) and used to amplify specific target genes with the Takyon SYBR Green according to manufacturer's instructions (Eurogentec, Liège, Belgium) in the Light Cycler 96 real-time polymerase chain reaction system (Roche Diagnostics, Mannheim, Germany). Primer sequences are listed

in Table 2. Relative gene expression was computed using the  $2^{-ddCq}$  method with HPRT as housekeeping gene.

## 2.10 | Western blot

Proteins were extracted from micro-dissected thalamus samples using a lysis buffer containing Tris-HCl pH 6.8 0.5 M, glycerol, sodium dodecyl sulfate 10% and dithiothreitol 200 mM. Samples were boiled at 100°C for 5 min and then centrifuged at 4°C at 10,000 rpm for 3 min. Protein concentration was measured using the Pierce protein assay kit (Thermo Scientific, Bleiswijk, Netherlands). Ten  $\mu$ g of



TABLE 3 Blood parameters

	Normonatremia (mEq/L)	Hyponatremia	ODS 24 hr	$\Delta\text{SNa}^+$ 24 hr
$\text{Na}^+$	144 $\pm$ 8	106 $\pm$ 10 ***	142 $\pm$ 8###	33 $\pm$ 7
$\text{K}^+$	4.9 $\pm$ 0.77	7.7 $\pm$ 1.8 ***	7.4 $\pm$ 1.3***	0.3 $\pm$ 2.3
$\text{Cl}^-$	122 $\pm$ 9	80 $\pm$ 14***	125 $\pm$ 11###	42 $\pm$ 10

\*\*\* $p < .001$  compared with normonatremia, ### $p < .001$  compared with hyponatremia, mean  $\pm$  SD.

proteins were loaded on a 4% stacking gel followed by a 10% running gel containing 40% of acrylamide for 1 hr at 120 V. Samples were then transferred on a PVDF membrane (Thermo Scientific, Bleiswijk, The Netherlands) for 1 h 30 min at 120 V. Membranes were incubated with a blocking solution containing 5% milk in TBS-Tween for 30 min and then with primary antibodies diluted in 5% milk in TBS-Tween at 4°C overnight. Primary antibodies used were anti-Cx43 (Abcam ab11370, 1:50,000), anti-Cx47 (Life Technologies #374500, 1:200), anti-cleaved caspase3 (Cell Signaling #9664, 1:1000). Membranes were then rinsed and incubated with an anti-rabbit or an anti-mouse HRP-linked antibody (Cell Signaling #7074S or #7076S) diluted 1:1000 in 5% milk in TBS-Tween. Signal was revealed using chemiluminescent method (Roche Diagnostics, Mannheim, Germany) and quantified on an Image Quant LAS 4000 mini (GE Healthcare, Diegem, Belgium). Loading control was performed using an anti- $\beta$ -actin antibody (Sigma #A5441) diluted 1:10,000 in 5% milk in TBS-Tween.

### 2.11 | BBB permeability

Evans Blue was intraperitoneally injected 1 hr before sacrifice. Animals were exsanguinated and transcardially perfused with NaCl 0.9%, until blood was fully withdrawn. Proencephalons were isolated, weighted before snap-freezing into liquid nitrogen, and then stored at  $-80^\circ\text{C}$  until analysis. Samples were thawed, digested in 250  $\mu\text{l}$  formamide for 3 days at  $65^\circ\text{C}$ . Next, samples were centrifuged at 13,000 rpm for 10 min at  $4^\circ\text{C}$  and supernatants analyzed with spectrophotometry at 620 nm. Dye concentration in the sample was interpolated from a standard curve and normalized with the wet weight of the tissue.

### 2.12 | Statistical analysis

Statistical analyses were computed using GraphPad Prism 5 software (GraphPad Software, La Jolla, CA, <http://www.graphpad.com>). Accounting for 58 mice included in ODS protocol with or without demyelinating lesions, a retrospective ROC curve analysis was obtained to prognosticate the risk of developing brain demyelination. Sensitivity, specificity, positive predictive value and negative predictive value were computed to determine the threshold values of hyponatremia and of  $\Delta\text{SNa}^+$  leading to the highest probability of developing ODS. Data were expressed as the mean  $\pm$  standard error of the mean (SEM) or relative quantification (RQ)  $\pm$  standard deviation (SD). Non-parametrical Kruskal–Wallis tests were performed to compare multiple groups and results were considered as significantly different for  $p < .05$ .

## 3 | RESULTS

### 3.1 | Blood parameters and neurological score during ODS protocol

Mice were subjected to ODS experimental protocol and monitored for blood parameters, neurological status and survival rate. During the phase of chronic hyponatremia (106  $\pm$  10 mEq/L vs. 144  $\pm$  8 mEq/L in normonatremic mice), mice did not present any obvious behavioral or physical abnormalities, except a slight weight loss. Modified levels of chloremia (80  $\pm$  14 mEq/L vs. 122  $\pm$  9 mEq/L,  $p < .001$ ) and kalemia (7.7  $\pm$  1.8 mEq/L vs. 4.9  $\pm$  0.77 mEq/L,  $p < .001$ ) were measured in hyponatremic mice (HN) compared with normonatremic mice (NN) (Table 3). Hyponatremia was corrected using a single bolus of hypertonic saline; 24 hr after the correction of hyponatremia, serum  $\text{Na}^+$  and  $\text{Cl}^-$  raised to normal values (142  $\pm$  8 mEq/L for  $\text{Na}^+$  and 125  $\pm$  11 mEq/L for  $\text{Cl}^-$ ). Hyperkalemia was still measured in corrected mice at 24 hr and lasted over time (7.4  $\pm$  1.3 mEq/L,  $p < .001$ ). 34% of corrected mice were found dead in their cages the day after correction, without having gotten the opportunity to measure their natremia. The mean 24-hr  $\Delta\text{SNa}^+$  for mice included in the study was 33  $\pm$  7 mEq/L (Table 3). Individual values of natremia are shown in Supporting Information, Figure S2. According to a retrospective ROC curve analysis (data not shown), we determined that mice with a chronic hyponatremia  $\leq 124$  mEq/L and a 24 hr  $\Delta\text{SNa}^+ \geq 27$  mEq/L at correction had the highest probability to develop demyelinating brain lesions. For these threshold values, we computed a sensitivity of 93.33%, a specificity of 92.86%, a positive predictive value of 93.33% and a negative predictive value of 92.86%. From 24 hr post-correction, most of mice presented obvious neurological symptoms such as gait paralysis or limb weakness, impairing significantly their neurological score (Figure 1a).

### 3.2 | ODS mice showed impairments of grip strength and auditory evoked potentials

Compared with normonatremic and uncorrected hyponatremic mice, corrected ODS mice showed lower muscular strength at 24 hr after the correction. Surprisingly, ODS mice at 48 hr after the correction presented no statistically relevant differences (Figure 1b). As ODS has previously been described to affect white matter tracts along the auditory pathway in human cases, we measured BAEPs before and after correction of hyponatremia. ODS mice showed significant lower amplitudes for waves III and V at 24 hr after the correction (Figure 1d), together



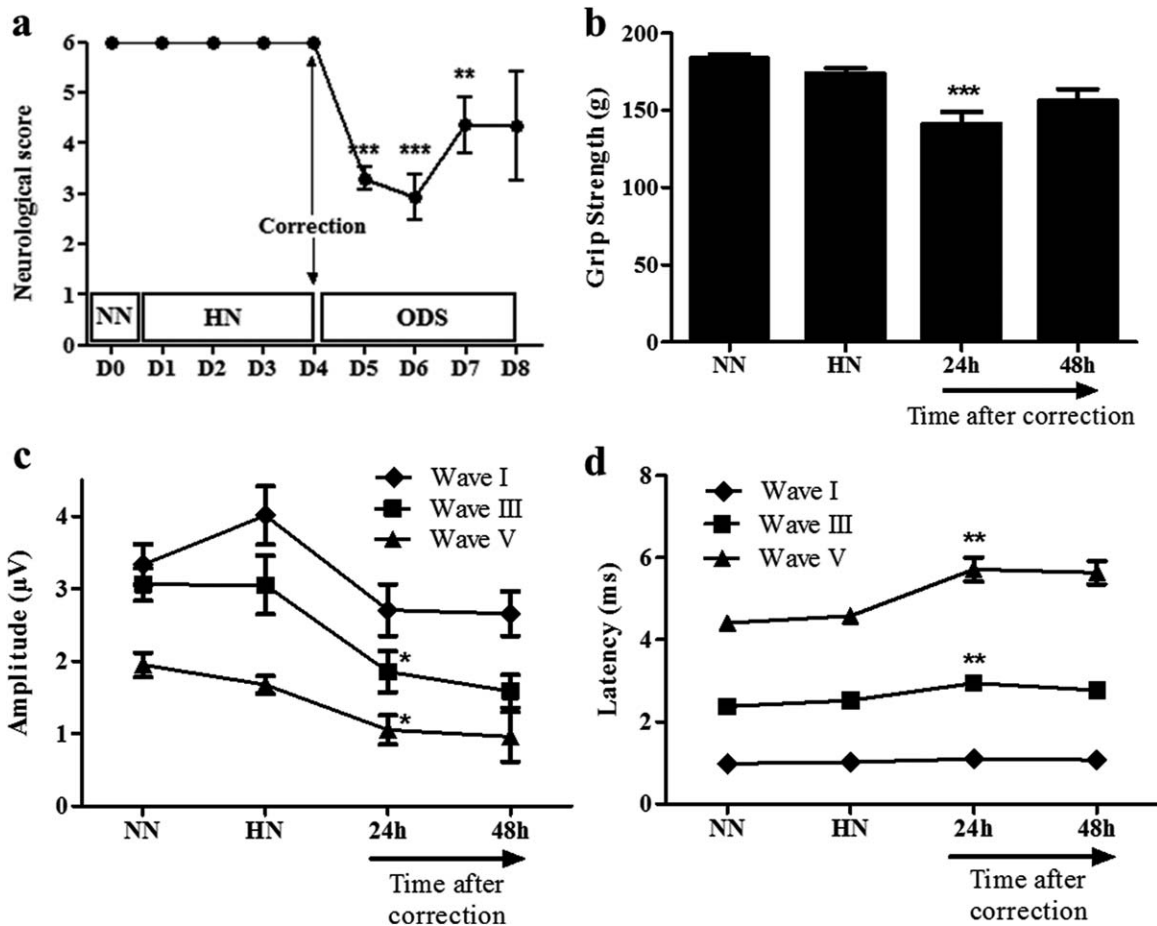


**FIGURE 1** Neurologic and functional changes in ODS mice. Neurological score decreased from 24 to 72 hr after the correction of hyponatremia. Surviving ODS mice showed partial recovery from 72 hr to latter time point (a) (\*\* $p < .01$ ; \*\*\* $p < .001$ , Kruskal–Wallis test, D0  $n = 30$ , D1  $n = 30$ , D2  $n = 30$ , D3  $n = 30$ , D4  $n = 30$ , D5  $n = 30$ , D6  $n = 30$ , D7  $n = 14$ , D8  $n = 6$ ). Normonatremic mice (NN) and chronic uncorrected hyponatremic mice (HN) showed no deficit in muscle strength. Grip strength was significantly impaired at 24 hr post-correction in ODS mice (b) (\*\* $p < .001$  vs. NN group, Kruskal–Wallis test, NN  $n = 13$ , HN  $n = 13$ , 24 hr  $n = 13$ , 48 hr  $n = 5$ ). For brainstem auditory evoked potentials (BAEPs), the amplitudes of waves I, III, and V were slightly decreased in ODS mice after correction (c). The latency of waves III and V (analysis between peaks I and III and between peaks I and V) was significantly delayed at 24 hr after correction in ODS compared with NN mice (d) (\* $p < .05$ , \*\* $p < .01$ , Kruskal–Wallis test, NN  $n = 12$ , HN  $n = 12$ , 24 hr  $n = 12$ , 48 hr  $n = 4$ ). All data are expressed as mean  $\pm$  SEM

with higher latencies (Figure 1e). Peak I mostly results from the afferent action potential volley in the auditory nerve; peaks III–V are generated by brainstem structures caudal to the caudal colliculi. No differences were observed for amplitude or latency for wave I (Figure 1c,d).

### 3.3 | Demyelinating lesions were observed in ODS mice 48 hr after the correction of hyponatremia

Eriochrome Cyanine R staining on sagittal brain sections demonstrated striking loss of white matter in specific regions: cortex, thalamus, colliculus, and pons (Figure 2a). Each lesion is lined up with sharp boundaries (Figure 2b). No difference of myelin staining was observed between normonatremic and uncorrected hyponatremic mice. Myelin basic protein (MBP) immunohistochemistry confirmed myelin loss in same areas (Figure 2a). An exhaustive list of demyelinated brain regions is shown in Table 4. Thalamic nuclei, parietal associative cortex, secondary visual cortex, primary motor and somatosensory cortex were

the most damaged areas. Notably, substantial disorganization of the cortical myelin was often observed (Figure 2c). Demyelination was never detected in highly myelinated tracts such as the corpus callosum or the anterior commissure. Quantification of MBP immunolabelling showed that myelin was significantly lost at 48 hr after the correction, up to latter time points with about 8% of total prosencephalon area impacted (Figure 2d).

### 3.4 | Loss of oligodendrocyte and astrocyte markers, prior to demyelination

To unravel the mechanism of demyelination, we analyzed lesioned areas looking at the cells directly or indirectly involved in CNS myelination. The integrity of oligodendrocytes was first assessed because these cells are responsible for the CNS myelin formation and maintenance. In normonatremic and hyponatremic mice, numerous APC<sup>+</sup> oligodendrocytes were counted in the thalamus. After correction of

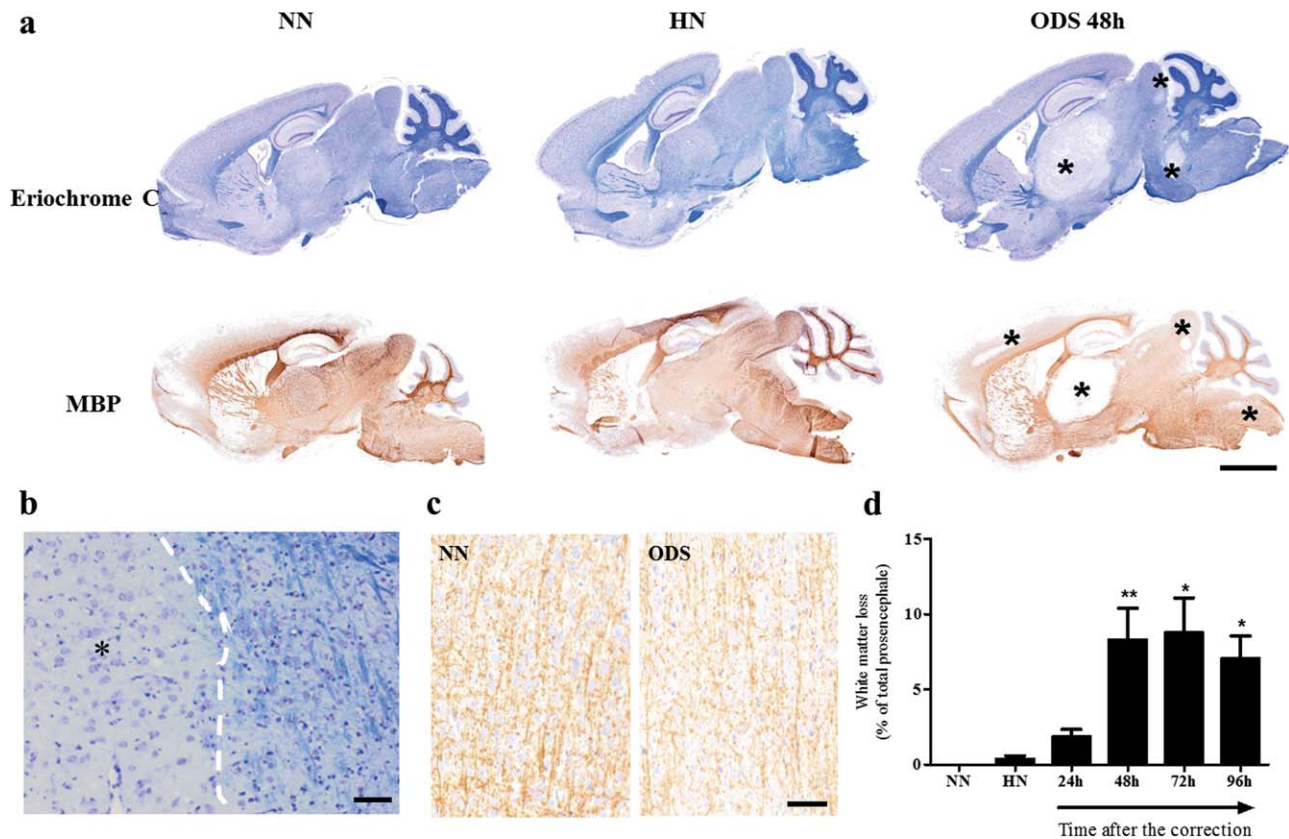


**FIGURE 2** Demyelination and myelin disorganization in specific-brain regions. In ODS mice, cortex, thalamic nuclei, inferior colliculus and pontine nuclei were the most frequent regions damaged. Alterations in white matter content were evidenced in sagittal brain sections by using Eriochrome C and confirmed by MBP immunolabeling (a). A high magnification of a demyelinating lesion in the thalamus exemplifies its clear delineation among the remaining midbrain region (b). In ODS mice, MBP immunolabeling illustrates the cortical myelin disorganization (right) compared with normonatremic mice (left) (c). No myelin defect can be found in both NN and HN mice. Quantification of MBP-immunoreactivity of the prosencephalon sections showed a significant myelin loss at 48 hr point after the correction compared with NN (d) (\* $p < .05$ , \*\* $p < .01$ , Kruskal-Wallis test, NN  $n = 5$ , HN  $n = 4$ , 24 hr  $n = 9$ , 48 hr  $n = 5$ , 72 hr  $n = 4$ , 96 hr  $n = 5$ ). Results are expressed as mean + SEM. Scale bars = 2 mm in a and 20  $\mu\text{m}$  in b and c

chronic hyponatremia, APC immunoreactivity dropped drastically (Figure 3a). A significant reduction of APC<sup>+</sup> labeled cells was identified at 24 hr after the correction, which is also 24 hr before any significant myelin loss (Figure 3b). Loss of p25 $\alpha$ <sup>+</sup> oligodendrocytes in thalamus corroborated loss of APC immunoreactivity (data not shown). Furthermore, a double immunolabeling for myelin and oligodendrocytes (Figure 3c) at the same time-point confirmed oligodendrocytopathy prior to myelin loss. At 48 hr post-correction, the injury to oligodendrocytes was spatially correlated to myelin loss in the thalamus and each other susceptible brain regions surveyed. In contrast, astrocytes are being functionally coupled to oligodendrocytes in the panglial syncytium. Loss of ALDH1L1 immunoreactivity, a specific astrocyte marker, was detected in same susceptible brain regions within 24 hr after the osmotic injury (Figure 3d,f). The regional damages coincided spatially and temporally with the regions that are impacted by demyelination, as attested by double immunolabeling MBP/ALDH1L1 and SMI94/ALDH1L1 (Figure 3d–f). Loss of other astrocyte markers such as AQP4 and S100 $\beta$  corroborated temporally and spatially ALDH1L1 immunohistochemical results (data not shown). Morphology of ALDH1L1 astrocytes was followed up from 6 hr post-correction to late time

points and revealed early clasmatodendrosis (Supporting Information, Figure S3).

### 3.5 | Dysregulation of astrocytes/oligodendrocytes (A/O) gap junctions

In ODS brains, less Cx47<sup>+</sup> cells were counted in the thalamus than in hyponatremic brains (Figure 4a,b). Although Cx47 protein expression showed no obvious difference between groups (Figure 4c), expression of Cx47 mRNA showed a trend to decrease at 24 hr after the correction (Figure 4d). In brain slices, Cx43 immunoreactivity decreased at 24 and 48 hr after the correction of hyponatremia (Figure 4e,f). This latter change was correlated with a downregulation of Cx43 protein (Figure 4g) and gene expression (Figure 4h).

### 3.6 | Osmotic injury leads glial cells toward necroptosis in ODS lesions

At the ultrastructural level, the thalamus of ODS mice at 12 hr post-correction demonstrated that most oligodendrocytes were more

TABLE 4 Topographical distribution of demyelinating lesions

Extrapontine regions	Percentage of ODS mice (%)
Thalamic nuclei	100
Lateral and medial parietal association cortex	64
Secondary visual cortex	47
Primary motor cortex	42
Secondary motor cortex	36
Primary somatosensory	36
Ventral posteromedial thalamic	39
Posterior thalamic nuclear group	36
Ventrolateral thalamic nucleus	31
Lateral postthalamic nucleus, mediorostral	17
Laterodorsal thalamic nucleus, ventrolateral	17
Central nucleus of inferior colliculus	14
Cuneiform nucleus	11
Centro-pontine regions	
Superior cerebellar peduncle	11
Lateral parabrachial nucleus	8
Medial parabrachial nucleus	8
Pedunculotegmental nucleus	8

electron-contrasted than that of uncorrected mice. Many showed obvious changes, such as nuclear and cytoplasmic features that suggest irreversible injuries (toward a form of cell death). The damaged oligodendrocytes showed intensely-contrasted nucleus with chromatin hypercondensation, degradation of the nucleolus marked by interchromatin granules. Most of the injured cells showed poorly demarcated or total loss of nuclear membrane, and cytoplasmic vacuolization (Figure 5a). All these changes were absent in normonatremic controls. The most damaged cells identified were the oligodendrocytes and secondarily the astrocytes that revealed nuclear hyperchromaticity accompanied by swollen organelles and autophagocytoses at 48 hr after the correction (Figure 5a). Further investigations to clarify the cell death underlying this gliopathy were carried out. The apoptosis pathway was first explored using cleaved caspase 3 assay and TUNEL method. No cleaved caspase 3 signal was detected in any brain protein extract at 24 hr after the correction, although positive control was included and revealed a specific band at 17kDa (Figure 5b). This absence of apoptotic cascade activation was further confirmed on ODS brain slices using a fluorescent TUNEL-based assay, cleaved caspase 3 and gamma H2AX immunolabelings including appropriate positive controls (data not shown). In-depth analysis of TEM samples never showed the presence of apoptotic cells/bodies in the thalamus at either 12 or 48 hr post-correction (data not shown). Next, the necroptosis pathway was

investigated using immunohistochemistry targeting the downstream effector of the necroptotic cascade, MLKL and its active phosphorylated form (p-MLKL). Immunohistochemistry against p-MLKL revealed strong immunoreactivity in and around lesioned brain areas of ODS mice, which was never observed in normonatremic or hyponatremic mice (Figure 5c). In the thalamus, pMLKL immunoreactivity was detected at the level of the plasma membrane and the nucleus of degenerating glial cells as well as along nerve fibers (Figure 5c).

### 3.7 | Expression changes of myelinotoxic and pro-myelinogenic factors

We performed qRT-PCR on several genes involved into cellular death (TNFRSF6 and FasL), neuroinflammation (IL-1 $\beta$  and TNF $\alpha$ ), and myelination (MBP, PLP1, CNP1, LIF, GDNF, and BDNF). TNFRSF6 mRNA and FasL gene expressions were upregulated (Figure 6a,b) in the thalamic ODS samples. Although there was no statistically difference for pro-inflammatory TNF $\alpha$  mRNA expression (Figure 6c), the IL-1 $\beta$  mRNA relative expression was highly upregulated (Figure 6d). No changes in MBP, GDNF and BDNF mRNA expression were measured (Figure 6e,i, j), while relative PLP1 mRNA expression was decreased at 48 hr after the correction (Figure 6f). CNP1 mRNA relative expression was down-regulated at 24 hr after the correction (Figure 6g). LIF mRNA levels were increased in ODS samples at 48 hr after the osmotic correction (Figure 6h).

### 3.8 | BBB disruption was observed 48 hr after the correction of hyponatremia

IgG immunoreactivity was not detected in the brain parenchyma from normonatremic and hyponatremic mice (data not shown). Inversely, at 48 hr after the correction, considerable IgG leakages were observed in thalamic nuclei and in other demyelinated areas, otherwise still absent 24 hr after the correction (Figure 7a). Similarly, amounts of extravasated Evans Blue were significantly increased at 48 hr post-correction in the brain extract of ODS mice, comforting the BBB disruption at that timing (Figure 7b). Mice included in Evans Blue assay and euthanized at 24 hr and 48 hr after the correction had respectively a  $\Delta$ SNa<sup>+</sup> of 36 and 28 mEq/L. To seek for microbleeds in ODS brains, slices were stained with Perls' method but they never revealed the presence of hemosiderin deposits after careful inspection of all the sections prepared (data not shown).

### 3.9 | Early microglial activation in ODS mice

In normonatremic and hyponatremic mice, quiescent Iba1<sup>+</sup> microglial cells were observed throughout the brain. They presented a ramified morphology typical of a resting state, namely type A (Figure 8a,b). In case of activation, cellular ramifications retract, cells become hypertrophied, progressively turning into an amoeboid phenotype or type D (Figure 8b). The microglial morphology changes were quantified in the thalamus and changed toward a type B morphology within 24 hr after the correction (Figure 8a-c) and even at 12 hr post-correction (data not shown). At the later time points, majority of type C and type D cells



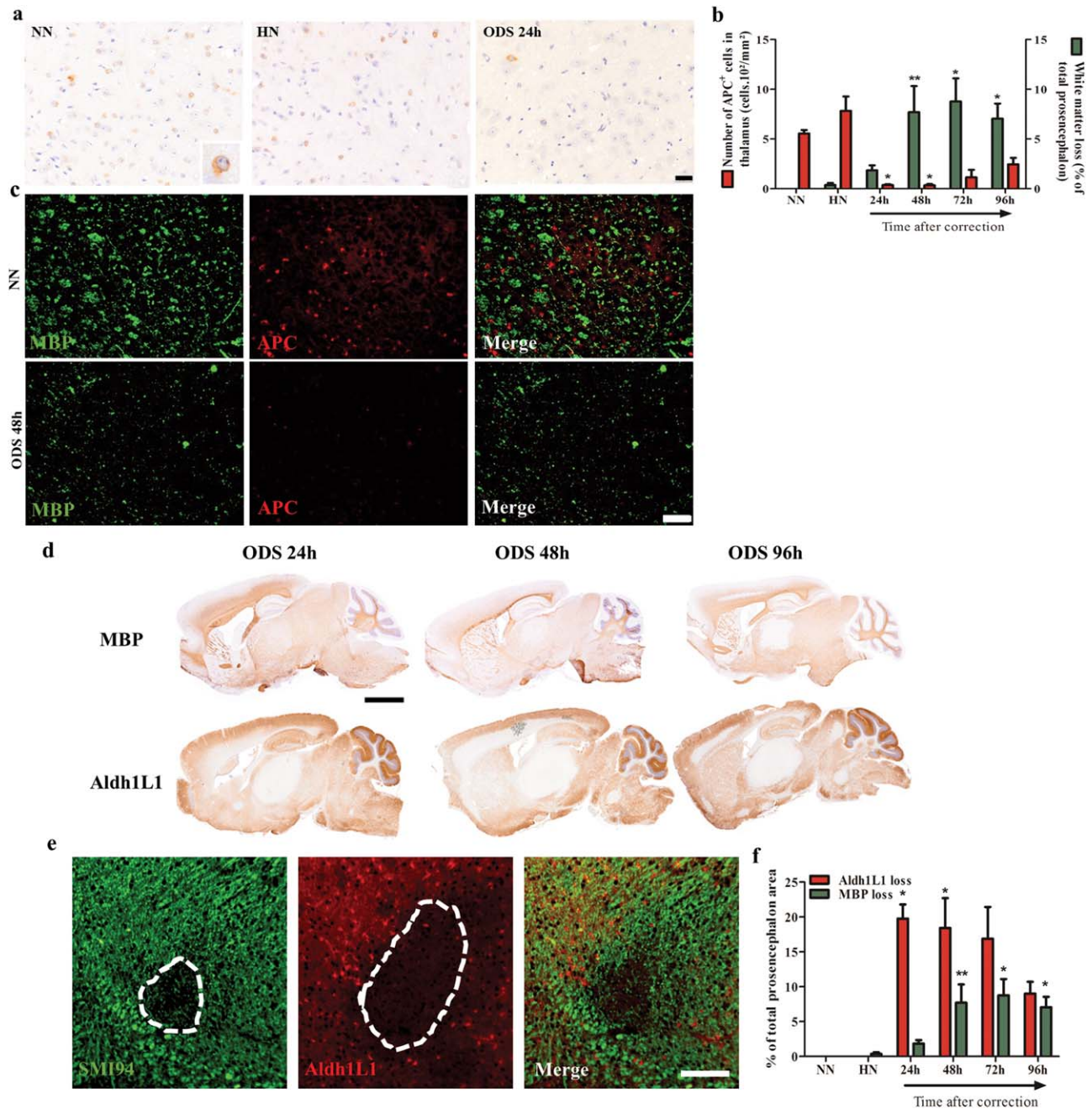


**FIGURE 3** Oligodendrocytopathy and astrocytopathy, prior to demyelination. APC-immunoreactivity was decreased in lesioned brain areas (a). This observation was confirmed by the quantification of APC<sup>+</sup> cells in the thalamus (b). Loss of APC<sup>+</sup> cells started at 24 hr after the correction (red bars in b) whereas significant myelin loss started at 48 hr post-correction (green bars in b) ( $*p < .05$ ,  $**p < .01$ , Kruskal–Wallis test, NN  $n = 8$ , HN  $n = 7$ , 24 hr  $n = 5$ , 48 hr  $n = 4$ , 72 hr  $n = 4$ , 96 hr  $n = 5$ ). A double immunolabeling in the thalamic nuclei at 48 hr post-correction demonstrated that APC<sup>+</sup> oligodendrocytes (red) are lost in the same area affected by myelin disruption (green) (c). Aldh1L1, as astrocyte marker (bottom) is depleted in the same brain areas devoid of MBP immunoreactivity (top) (d–e). At 24 hr post-correction, myelin SMI94 immunolabeling (green in e) and Aldh1L1 (red in e) superimposed the loss of astrocytes of the same demyelinating lesion. In ODS mice, the quantification of Aldh1L1-immunoreactivity in the prosencephalon showed a significant decrease at 24 hr post-correction point and at latter time points when compared with NN (f) ( $*p < .05$ ,  $**p < .01$ , Kruskal–Wallis test, NN  $n = 5$ , HN  $n = 5$ , 24 hr  $n = 5$ , 48 hr  $n = 4$ , 72 hr  $n = 4$ , 96 hr  $n = 5$ ). Data are expressed as mean + SEM. Scale bars = 20  $\mu\text{m}$  in a, 50  $\mu\text{m}$  in c, 2 mm in d, and 200  $\mu\text{m}$  in e

were observed (Figure 8b,c). While activated microglial cells were evenly distributed in the epicenter of the demyelinating lesions, Iba1<sup>+</sup> cells appeared to move to a more peripheral distribution at the late

time points. Except for a slight decrease at 24 hr after the correction, the density of thalamic Iba1<sup>+</sup> cells was not different among the experimental groups (Figure 8d).

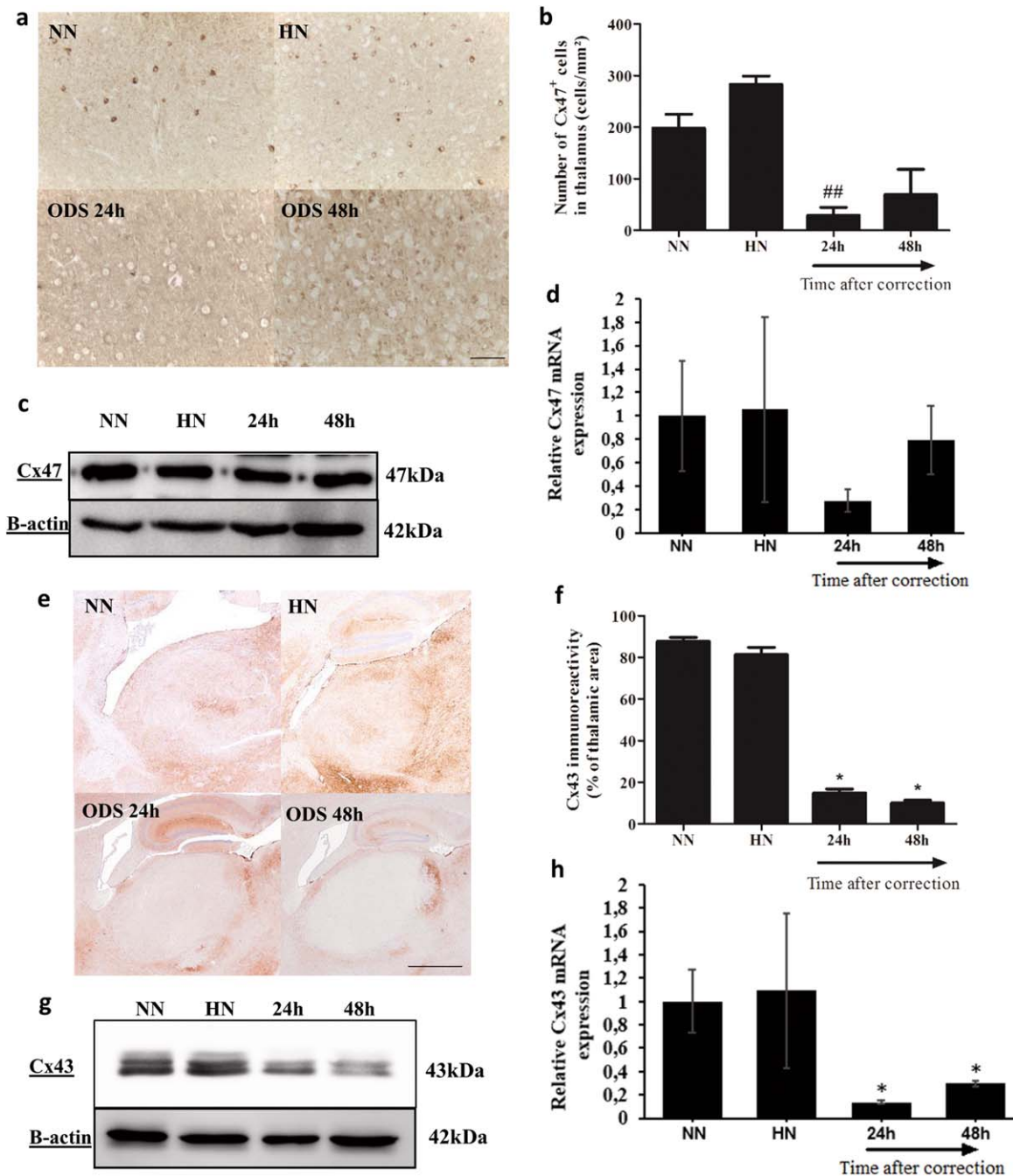


**FIGURE 4** Astrocyte-oligodendrocyte gap junctions in ODS mice. Cx47<sup>+</sup> immunoreactivity revealed a diminution of thalamic Cx47<sup>+</sup> cells (a) This depletion is significantly different at 24 hr after the correction, compared with uncorrected hyponatremic (HN) mice (b). Cx47 protein Western blots analyses revealed no difference between groups (c). Relative analysis of Cx47 mRNA was not significantly changed despite a trend toward diminution at 24 hr after the correction (d). Cx43-immunoreactivity decreased in thalamic nuclei after the correction (e). The quantification of Cx43 immunoreactivity showed a significant reduction at 48 hr after the correction, while a non-statistically diminution was already observed at 24 hr after the correction (f). Cx43 protein Western blot analyses also showed a sharp decrease after the correction (g) and the mRNA transcripts confirmed the downregulation of Cx43 expression (h) (\**p* < .05 compared with NN, ##*p* < .01 compared with HN, Kruskal-Wallis test, NN *n* = 4, HN *n* = 4, 24 hr *n* = 6, 48 hr *n* = 3). Results are expressed as mean + SEM in (b) and (f). mRNA results in (d) and (h) are expressed as RQ ± SD. Scale bars = 500 μm in a and 50 μm in e

## 4 | DISCUSSION

Following rapid correction of chronic hyponatremia, mice recapitulated the neurological symptomatology and the histological changes

observed in the rat model or even in human pathology. Based on retrospective data analysis of this mouse model, we determined that levels of hyponatremia  $\leq 124$  mEq/L and a 24-hr  $\Delta\text{SNa}^+ \geq 27$  mEq/L give the maximal likelihood of developing pathognomonic ODS brain lesions in



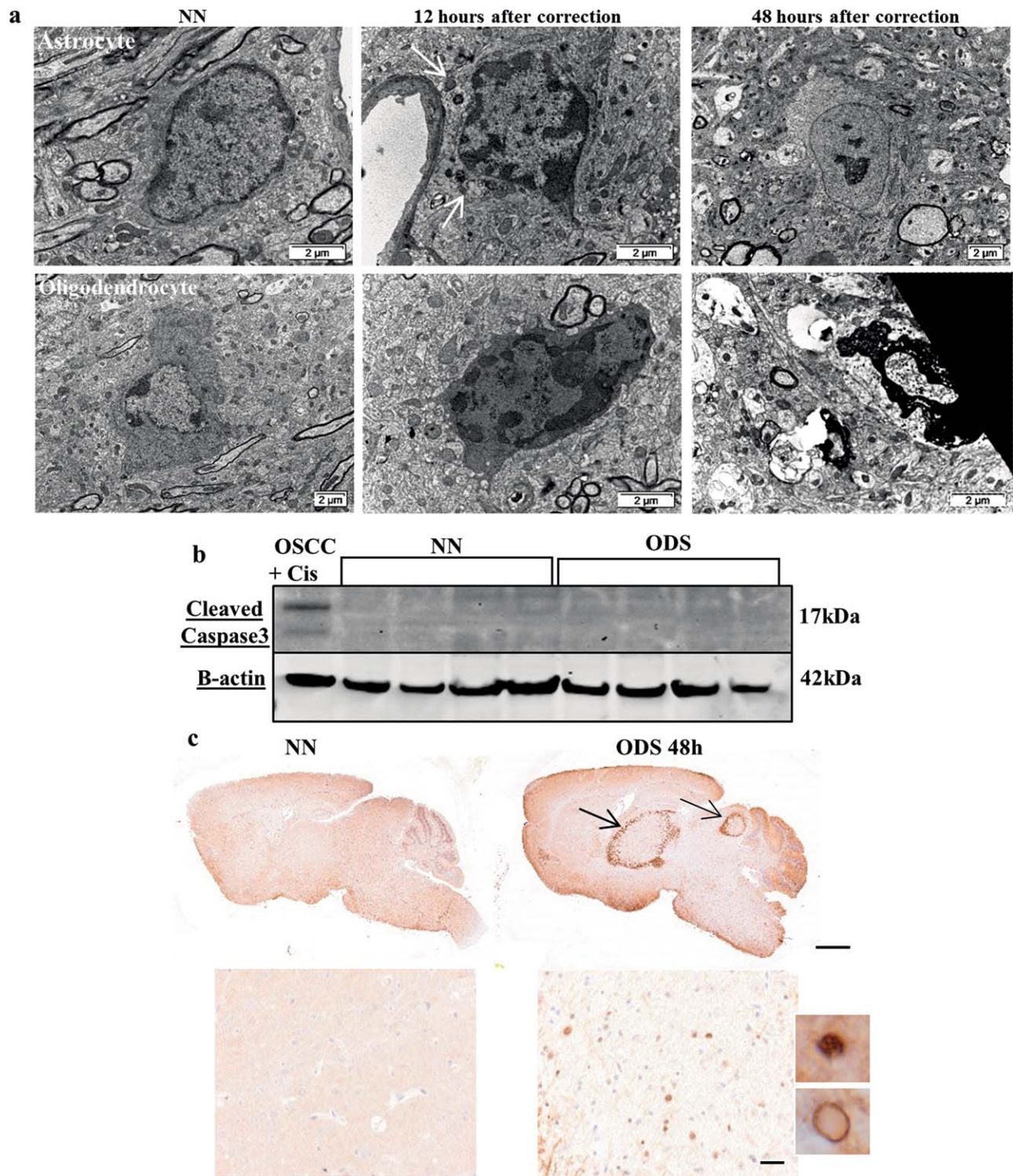


**FIGURE 5** Necroptosis-dependent glial cell injuries in ODS lesions. 12 hr post correction, electron microscopy revealed chromatin hypercondensation and nucleolar changes in astrocytes and oligodendrocytes. At this time-point, myelin sheaths are not yet disrupted in ODS brains but glial cells showed autophagocytosis (white arrows). However, 48 hr after the correction, oligodendrocytes demonstrated stronger nuclear degradation than astrocytes (a). Cleaved caspase 3 was not detected in thalamic ODS samples (b) suggesting that apoptosis is not implicated in oligodendrocyte or astrocyte death. However, p-MLKL, a downstream effector of the necroptosis pathway demonstrated a strong immunoreactivity in and around lesioned areas (c, black arrows). pMLKL immunoreactivity appeared localized in the nucleus and on the neurolemma of many thalamic glial cells of ODS mice (inset). Scale bars = 1 mm in c (top) and 500 μm in c (bottom) [Color figure can be viewed at [wileyonlinelibrary.com](http://wileyonlinelibrary.com)]

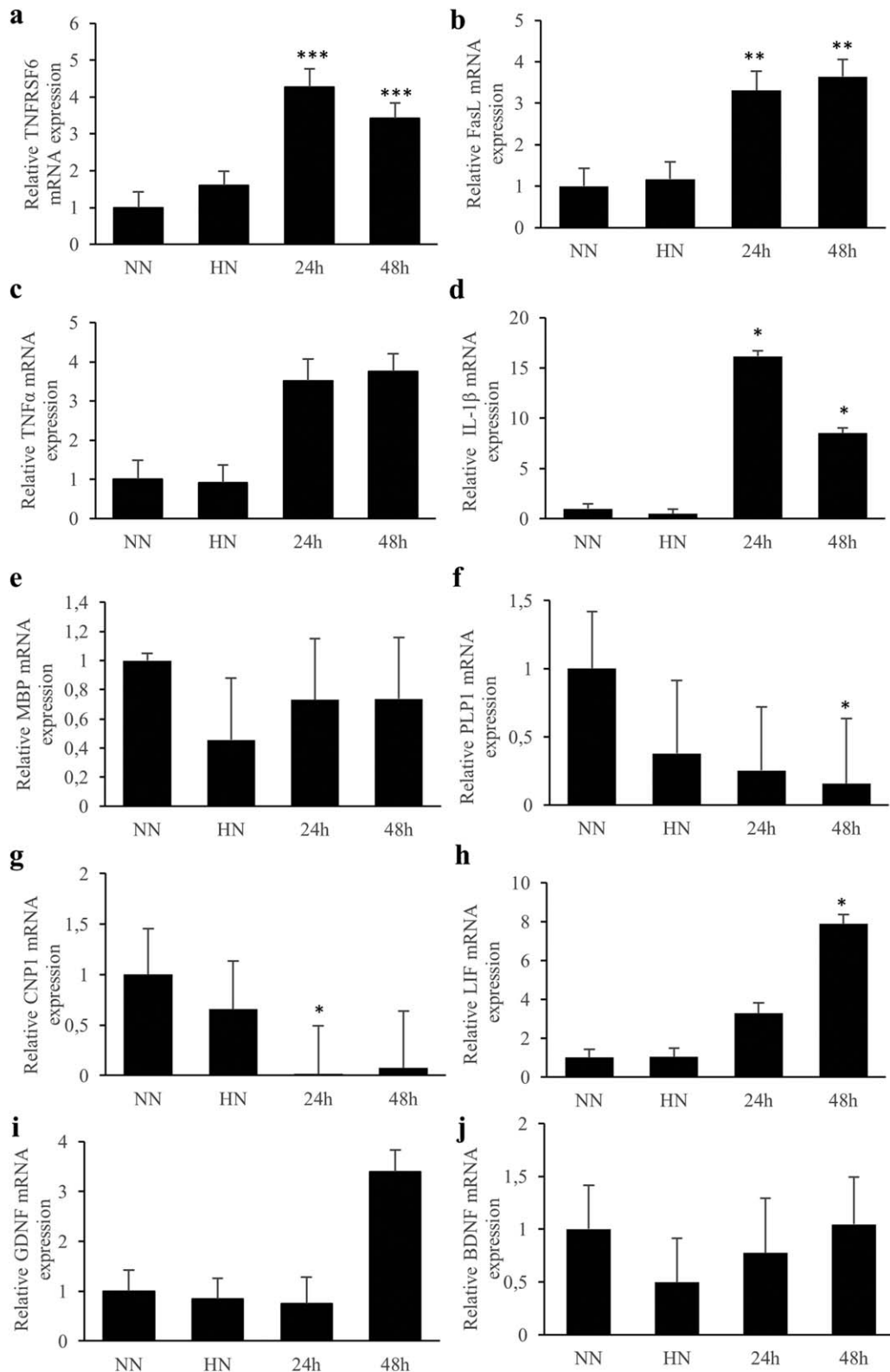


**FIGURE 6** Gene expression of myelinotoxic (TNFRSF6, FasL, TNF $\alpha$ , and IL-1 $\beta$ ) and promyelogenic (MBP, PLP1, CNP1, LIF, GDNF, and BDNF) factors. No differences were observed between normonatremic mice (NN) and hyponatremic mice (HN) for any of the genes analyzed. TNFRSF6 and FasL mRNA expressions were significantly increased after the correction compared with NN (a and b). An increasing trend of TNF $\alpha$  was observed (c) whereas a significant increase for IL-1 $\beta$  mRNA expression occurred after the correction compared with NN (d). No difference between experimental groups for MBP (e), GDNF (i), and BDNF (j) were observed. PLP1 mRNA expression was statistically downregulated at 48 hr after the correction compared with NN (f). CNP1 mRNA levels were significantly downregulated at 24 hr after the correction compared with NN (g). LIF mRNA was significantly upregulated at 48 hr after the correction compared with NN (h) (\* $p < .05$ , \*\* $p < .01$ , \*\*\* $p < .001$ , Kruskal-Wallis test, NN  $n = 5$ , HN  $n = 5$ , 24 hr  $n = 9$ , 48 hr  $n = 5$ ). Results are expressed as RQ + SD

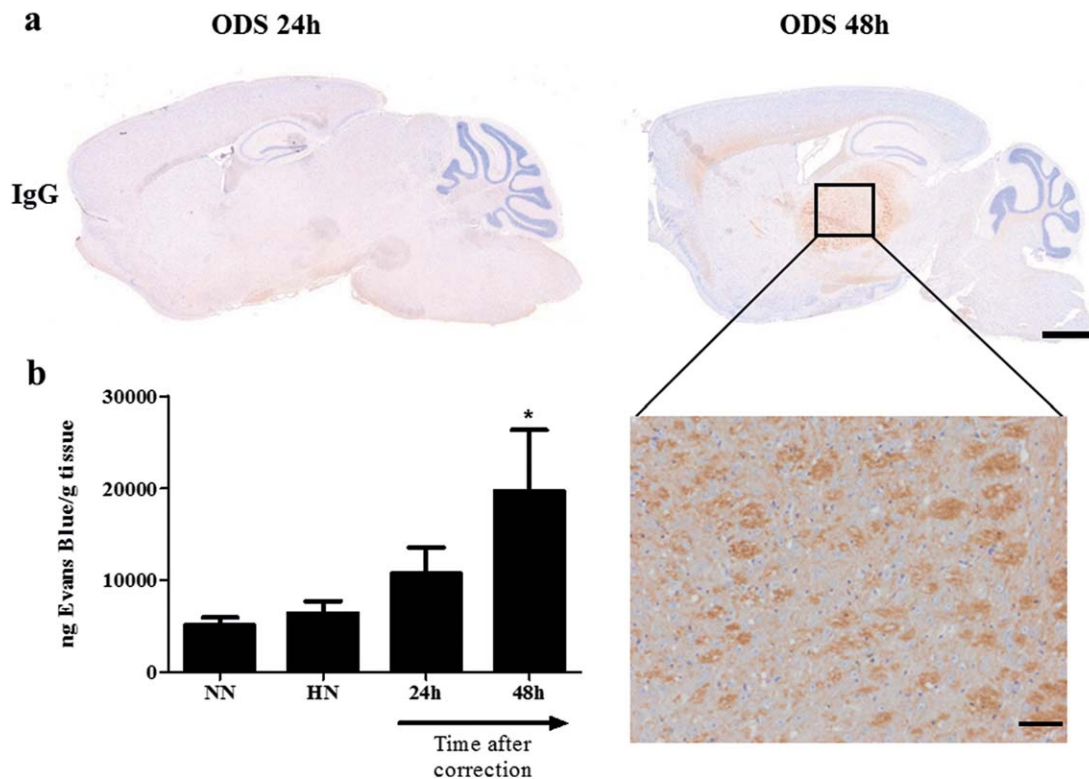


**FIGURE 7** Assessment of blood–brain barrier permeability in ODS brains. Brain tissue IgG extravasation was detected at 48 hr post-correction (a). The brain regions most immunoreactive for anti-mouse IgG included the thalamus and the subcortical regions. Similarly, significant Evans Blue extravasation was measured at 48 hr post-correction point in whole-brain homogenates from ODS mice compared with NN (b). Noteworthy,  $\Delta\text{SNa}^+$  for 24 hr group and 48 hr group were not different (36 and 28 mEq/L, respectively). (\* $p < .05$ , Kruskal–Wallis test, NN  $n = 7$ , HN  $n = 5$ , 24 hr  $n = 7$ , 48 hr  $n = 7$ ). Results are expressed as mean + SEM. Scale bars = 1 mm and 500  $\mu\text{m}$  in inset

mice. These values are close to those described in previous studies conducted in rats (Soupert, Stenuit, Perier, & Decaux, 1991). Noteworthy, hemolysis was often observed after tail blood sampling, which could explain unexpected higher levels of  $\text{K}^+$ . In this murine model, 34% of the mice died within the first day post-correction, whereas all the surviving mice invariably developed neurological manifestations of ODS, including sensory-motor deficits. In correlation with the functional impairments, myelin disorganization and loss were noted in related-brain areas, such as the pons, thalamic nuclei, inferior colliculus and cortical regions, consistent with human ODS lesion topography (Martin, 2004). In this mice study, no lesions were detected in the hippocampus, cerebellum or putamen although these regions are impacted in human ODS. This discrepancy can be explained by species-specific cellular response to the correction of hyponatremia or alternatively by the differential content of susceptible brain regions. For instance, in ODS rat model, demyelinating lesions were rarely identified in the pons, although they are found in human patients and in the mouse model. This observation could be explained by comparable cyto- and myelo-architectures of murine and human pons, composed of an admixture of grey and white matters (Lindquist et al., 2016).

In our ODS mice model, the significant nuclear damages (chromatin condensation, loss of nucleolus and nuclear membrane disappearance) along with other deteriorating injuries found in most

oligodendrocytes and some of the astrocytes of the susceptible brain regions, prior to demyelination corroborate the morphological losses of glial cell markers. These pathological events at cellular level prefigured myelin deterioration at 48 hr post-correction but also some aspects of glial cell death. Evidences of oligodendrocytic apoptosis were observed in human ODS samples (DeLuca et al., 2002) and in ODS rats (Gankam Kengne et al., 2011; Rojiani, Cho, Sharer, & Prineas, 1994). Moreover, in the rat model, astrocytes undergo apoptosis before oligodendrocyte or myelin loss (Gankam-Kengne, Couturier, Soupert, Brion, & Decaux, 2017; Gankam Kengne et al., 2011). We failed to replicate these findings in ODS mice as TUNEL assay, immunohistochemistry against cleaved caspase 3 and gamma H2AX; furthermore, anti-cleaved caspase 3 western blots were negative in lesioned brain areas. Given the upregulation of Fas (TNFRSF6) and FasL expression, it is hypothesized that an alternative mechanism can be responsible for the glial cell deaths. The phosphorylated form of MLKL, one of the effectors of the necroptosis, was highly expressed in the demyelinated brain regions. It has been demonstrated that binding of FasL onto its receptor Fas could switch on the necroptotic cascade when caspase 8-mediated pathway is inhibited. This cascade, culminates with the phosphorylation, the oligomerization of MLKL and its translocation to the plasma membrane where it provokes cytotoxic calcium influx through TRPM7 cation channel (Cai et al., 2014; Vanden Berghe, Linkermann, Jouan-Lanhuet, Walczak, & Vandenabeele, 2014). Phosphorylated MLKL



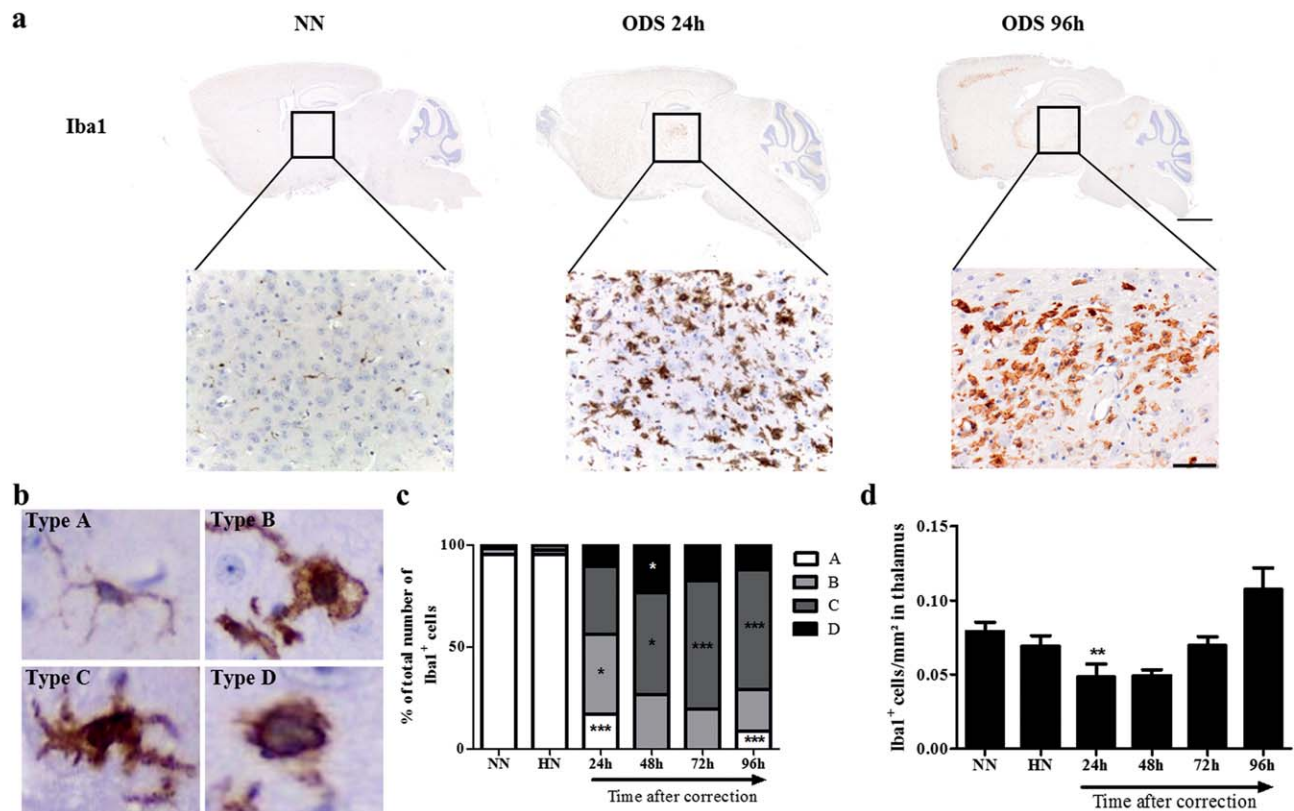


**FIGURE 8** Microglial activation, proliferation and distribution in ODS lesions. Iba1<sup>+</sup> microglial cells were tiny sized, highly ramified and sparsely distributed similarly in normonatremic (NN) and hyponatremic (HN [not shown]) mice brains (a). Iba1<sup>+</sup> cells were randomly distributed in early brain lesions, such as 24 hr post-correction, but appear to encircle like a demarcation of the lesion core at 96 hr (upper panels). Classification of thalamic Iba1<sup>+</sup> microglial cells was made according to four morphological types, from a ramified type A to type D, amoeboid (b). As soon as 24 hr post-correction, thalamic Iba1<sup>+</sup> cells underwent morphological changes toward a type B microglia (a). The number of type C and type D microglial cells increased from 24 hr onwards to 48 hr, while C type increased, D type reduced at 72 hr and 96 hr post-correction points in ODS mice (c). Compared with NN, the number of thalamic Iba1<sup>+</sup> microglial cells was transiently decreased at 24 hr post-correction but did not differ significantly with NN and HN brains at the later time-points of comparison (d). (\* $p < .05$ , \*\* $p < .01$ , \*\*\* $p < .001$ , Kruskal-Wallis test for each type, NN  $n = 3$ , HN  $n = 4$ , 24 hr  $n = 6$ , 48 hr  $n = 4$ , 72 hr  $n = 3$ , 96 hr  $n = 6$  mice). Data are expressed in (d) as mean + SEM. Scale bars = 1 mm and 50  $\mu$ m in insets [Color figure can be viewed at [wileyonlinelibrary.com](http://wileyonlinelibrary.com)]

also translocates to the nucleus but the downstream effects are not known (Yoon, Bogdanov, Kovalenko, & Wallach, 2016).

It is well established that oligodendrocytes and astrocytes act together to support myelin maintenance (Domingues, Portugal, Socolato, & Relvas, 2016; Tress et al., 2012) and the functions of the pial syncytium. Astrocytes and oligodendrocytes are chemically connected to each other by heterotypic A/O gap junctions established mostly by Cx43 and Cx47, although Cx30/Cx32 channels are also functional between those two cell types. Dysregulation of pial gap junctions causes demyelination, as demonstrated by connexin knock-down (KO) mouse models. KO of oligodendrocyte Cx47 results in myelin vacuolization whereas double genetic invalidation of astrocytic Cx30 and Cx43 unexpectedly provokes damages in oligodendrocytes and disruption of myelin sheaths (Li, Giaume, & Xiao, 2014; Lutz et al., 2009; Odermatt et al., 2003). In the thalamus of ODS mice, Cx43 and Cx47 expressions were both downregulated. Dysregulation of major A/O connexins could therefore participate in the local demyelination process. The survival of oligodendrocytes and myelination status also relies on trophic factors released from astrocytes (e.g., LIF, BDNF, and

GDNF; El Waly, Macchi, Cayre, & Durbec, 2014). An upregulation of LIF mRNA levels and a trend for elevated GDNF at 48 hr post-correction would originate from astrocytes that surround the demyelinated regions, in response to oligodendrocyte damages. The degradation of astrocytes, disruption of glial gap junctions or failure of trophic support in susceptible CNS regions might locally deplete the glial syncytium in myelinogenic factors and make local oligodendrocytes unable to sustain myelin integrity. As such, CNP1 mRNA, which encodes an essential oligodendrocyte enzyme, was downregulated at 24 hr after the correction. Despite the absence of differences in MBP mRNA expression, there was a significant decrease for PLP1 mRNA. Because the expression profile of MBP and PLP1 has not been investigated after 48 hr post-correction, one cannot rule out that cell repairs and remyelination occurs in the ODS brain lesions within days or weeks following the initial insult, as it is observed in lysoclethrin-induced demyelination (Woodruff & Franklin, 1999) or in experimental autoimmune encephalitis models (Mei et al., 2016).

Although ODS is not a primary inflammatory demyelinating disorder, the osmotic insult triggers a release of mediators of inflammation



that are able to exacerbate the glial cell damages (Iwama et al., 2011). Accordingly, we have measured an increased expression of IL-1 $\beta$  mRNA and a trend for increased TNF $\alpha$  mRNA levels during ODS in mice. Both cytokines, secreted by activated microglial cells and/or damaged astrocytes after injury (Choi, Lee, Lim, Satoh, & Kim, 2014; Didier et al., 2003), compromise oligodendrocyte survival (Su et al., 2011) or BBB impermeability (Argaw et al., 2006; Didier et al., 2003). In our study, BBB disruption is concomitant with myelin loss and delayed compared with glial cell loss, suggesting that BBB defect is not the primary event in ODS physiopathology, at least in mice. Furthermore, ODS could occur in rats without BBB opening (Gankam Kengne, Soupart, Pochet, Brion, & Decaux, 2009). In our model of ODS, resident microglial cells did not proliferate following the osmotic insult but switched rapidly into an activated phenotype within the first hours. This modification means that either these cells are able to sense the osmotic changes itself or they can respond to some damage-associated molecular patterns released from injured glial cells. Unlike the brains of rats and humans in which microglial activation is usually described in late ODS lesions (Adams et al., 1959; DeLuca et al., 2002; Popescu et al., 2013), morphological changes in murine microglia were noted as early as 12 hr post-correction. So far, the trigger for the microglial activation is not known. Their early activation, associated with the release of inflammatory mediators suggests an active role in glial cell or myelin damages. As previously shown, administration of minocycline, an inhibitor of microglial activation, decreased brain demyelination in the rat model of ODS (Gankam-Kengne et al., 2010; Suzuki et al., 2010; Takagi et al., 2014). In a more subtle way, it has been proposed that microglia could play a detrimental role in the early phase of ODS fostering brain inflammation but could turn into a protective phenotype during later phases by secreting trophic factors (Iwama et al., 2011).

As previously demonstrated in rats undergoing correction of a chronic hyponatremia, the re-integration of organic osmolytes within different brain regions occurs at differential rates and the severity of demyelinating lesions inversely correlates with the local efficiency in replenishing osmolytes (Lien, 1995; Lien et al., 1991). Accordingly, the regional susceptibility to osmotic insult might be related to differential abilities for single glial cells to quickly (re-)accumulate organic osmolytes and/or to glial cell heterogeneity among the brain regions. For instance, astrocytes from hippocampus, cerebellum or retina all exhibit different regulatory volume responses (Hirrlinger, Wurm, Hirrlinger, Bringmann, & Reichenbach, 2008). Differences at the level of ion channels, transporters and receptors are increasingly reported among astroglial cells (Chatton, Magistretti, & Barros, 2016). Brain astrocytes differ in their profile of gap junction expression, with CNS regions expressing specific subtypes of connexins (Griemsmann et al., 2015). Astrocytes and oligodendrocytes gap junctions allow the passive diffusion of ions (Na<sup>+</sup>, K<sup>+</sup>, and Ca<sup>2+</sup>) or small molecules (sugars, amino acids, and ATP), supporting an ionic and metabolic sharing throughout the glial syncytium. Depending on the degree of coupling, differential abilities of controlling and distributing metabolic load might also explain the region-specific vulnerability to anisotonic conditions.

Consistent with previous results obtained in the rat ODS model, the correction of hyponatremia affected astrocyte viability during the

early phase of ODS in mice (Gankam-Kengne et al., 2017; Gankam Kengne et al., 2011). Morphological analysis in lesioned thalamus revealed clasmotodendrosis starting at 6 hr after the correction, reflecting astrocytic irreversible injury (Hulse, Winterfield, Kunkler, & Kraig, 2001). The active involvement of astrocytes into brain energy metabolism and ion homeostasis leads us to suspect a pivotal role of astrocytes during ODS (Chatton et al., 2016; Rose & Verkhratsky, 2016). Recently, one of us showed that astrocytes, but not oligodendrocytes, underwent severe defects in proteostasis, making of these cells a preferred target during the osmotic stress (Gankam-Kengne et al., 2017). If true, oligodendrocytes might be considered as collateral damages indirectly affected by regional astrocytopathy. Alternatively, the concept of oligodendrocyte heterogeneity throughout the CNS is emerging (Hardy, Lazzarini, Colman, & Friedrich, 1996; Marques et al., 2016) and would equally support the hypothesis of a region-specific oligodendrocyte vulnerability toward osmotic insult.

In conclusion, we successfully generated a mouse model of ODS characterized by early and regional astrocytopathy and oligodendrocytopathy, resulting from the rapid correction of a chronic hyponatremia. This gliopathy culminated with the activation of the necroptosis cascade and the loss of glial cells from the lesioned brain regions, prior to BBB disruption and demyelination. In addition, we showed that microglial cells are early activated in the course of ODS, possibly through direct or indirect signaling (i.e. osmotic stress, inflammatory stimuli, DAMPs) and that these cells could contribute to neuroinflammation. This model will allow the use of genetically modified mice for exploring the function of specific genes in the pathophysiology of ODS.

## ACKNOWLEDGMENT

Graphical abstract was designed using Motifolio(c) drawing toolkit.

## ORCID

Charles Nicaise  <http://orcid.org/0000-0001-9372-1496>

## REFERENCES

- Adams, R. D., Victor, M., & Mancall, E. L. (1959). Central pontine myelinolysis: A hitherto undescribed disease occurring in alcoholic and malnourished patients. *AMA Archives of Neurology and Psychiatry*, *81*, 154–172.
- Argaw, A. T., Zhang, Y., Snyder, B. J., Zhao, M. L., Kopp, N., Lee, S. C., ... John, G. R. (2006). IL-1 $\beta$  regulates blood–brain barrier permeability via reactivation of the hypoxia-angiogenesis program. *Journal of Immunology*, *177*, 5574–5584.
- Cai, Z., Jitkaew, S., Zhao, J., Chiang, H. C., Choksi, S., Liu, J., ... Liu, Z. G. (2014). Plasma membrane translocation of trimerized MLKL protein is required for TNF-induced necroptosis. *Nature Cell Biology*, *16*, 55–65.
- Chatton, J. Y., Magistretti, P. J., & Barros, L. F. (2016). Sodium signaling and astrocyte energy metabolism. *Glia*, *64*, 1667–1676.
- Choi, S. S., Lee, H. J., Lim, I., Satoh, J., & Kim, S. U. (2014). Human astrocytes: Secretome profiles of cytokines and chemokines. *PLoS One*, *9*, e92325.
- DeLuca, G. C., Nagy, Z., Esiri, M. M., & Davey, P. (2002). Evidence for a role for apoptosis in central pontine myelinolysis. *Acta Neuropathology*, *103*, 590–598.

- Didier, N., Romero, I. A., Creminon, C., Wijkhuizen, A., Grassi, J., & Mabondzo, A. (2003). Secretion of interleukin-1 $\beta$  by astrocytes mediates endothelin-1 and tumour necrosis factor- $\alpha$  effects on human brain microvascular endothelial cell permeability. *Journal of Neurochemistry*, *86*, 246–254.
- Domingues, H. S., Portugal, C. C., Socodato, R., & Relvas, J. B. (2016). Oligodendrocyte, astrocyte, and microglia crosstalk in myelin development, damage, and repair. *Frontiers in Cell and Developmental Biology*, *4*, 71.
- El Waly, B., Macchi, M., Cayre, M., & Durbec, P. (2014). Oligodendrogenesis in the normal and pathological central nervous system. *Frontiers in Neuroscience*, *8*, 145.
- Gankam-Kengne, F., Couturier, B. S., Soupart, A., Brion, J. P., & Decaux, G. (2017). Osmotic stress-induced defective glial proteostasis contributes to brain demyelination after hyponatremia treatment. *Journal of the American Society of Nephrology*, *28*(6), 1802–1813. <https://doi.org/10.1681/ASN.2016050509>.
- Gankam-Kengne, F., Soupart, A., Pochet, R., Brion, J. P., & Decaux, G. (2010). Minocycline protects against neurologic complications of rapid correction of hyponatremia. *Journal of the American Society of Nephrology*, *21*, 2099–2108.
- Gankam Kengne, F., Nicaise, C., Soupart, A., Boom, A., Schiettecatte, J., Pochet, R., ... Decaux, G. (2011). Astrocytes are an early target in osmotic demyelination syndrome. *Journal of the American Society of Nephrology*, *22*, 1834–1845.
- Gankam Kengne, F., Soupart, A., Pochet, R., Brion, J. P., & Decaux, G. (2009). Re-induction of hyponatremia after rapid overcorrection of hyponatremia reduces mortality in rats. *Kidney International*, *76*, 614–621.
- Griemsmann, S., Hoft, S. P., Bedner, P., Zhang, J., von Staden, E., Beinhauser, A., ... Steinhäuser C. (2015). Characterization of panglial gap junction networks in the thalamus, neocortex, and hippocampus reveals a unique population of glial cells. *Cerebral Cortex*, *25*, 3420–3433.
- Hardy, R. J., Lazzarini, R. A., Colman, D. R., & Friedrich, V. L. Jr. (1996). Cytoplasmic and nuclear localization of myelin basic proteins reveals heterogeneity among oligodendrocytes. *Journal of Neuroscience Research*, *46*, 246–257.
- Hirrlinger, P. G., Wurm, A., Hirrlinger, J., Bringmann, A., & Reichenbach, A. (2008). Osmotic swelling characteristics of glial cells in the murine hippocampus, cerebellum, and retina in situ. *Journal of Neurochemistry*, *105*, 1405–1417.
- Hulse, R. E., Winterfield, J., Kunkler, P. E., & Kraig, R. P. (2001). Astrocytic clasmotodendrosis in hippocampal organ culture. *Glia*, *33*, 169–179.
- Illowsky, B. P., & Lauren, R. (1987). Encephalopathy and myelinolysis after rapid correction of hyponatraemia. *Brain*, *110*(Pt 4), 855–867.
- Iwama, S., Sugimura, Y., Suzuki, H., Suzuki, H., Murase, T., Ozaki, N., ... Oiso Y. (2011). Time-dependent changes in proinflammatory and neurotrophic responses of microglia and astrocytes in a rat model of osmotic demyelination syndrome. *Glia*, *59*, 452–462.
- Kleinschmidt-DeMasters, B. K., & Norenberg, M. D. (1981). Rapid correction of hyponatremia causes demyelination: Relation to central pontine myelinolysis. *Science*, *211*, 1068–1070.
- Lauren, R. (1983). Central pontine myelinolysis following rapid correction of hyponatremia. *Annals of Neurology*, *13*, 232–242.
- Li, T., Giaume, C., & Xiao, L. (2014). Connexins-mediated glia networking impacts myelination and remyelination in the central nervous system. *Molecular Neurobiology*, *49*, 1460–1471.
- Lien, Y. H. (1995). Role of organic osmolytes in myelinolysis. A topographic study in rats after rapid correction of hyponatremia. *The Journal of Clinical Investigation*, *95*, 1579–1586.
- Lien, Y. H., Shapiro, J. I., & Chan, L. (1991). Study of brain electrolytes and organic osmolytes during correction of chronic hyponatremia. Implications for the pathogenesis of central pontine myelinolysis. *The Journal of Clinical Investigation*, *88*, 303–309.
- Lindquist, R. A., Guinto, C. D., Rodas-Rodriguez, J. L., Fuentealba, L. C., Tate, M. C., Rowitch, D. H., & Alvarez-Buylla, A. (2016). Identification of proliferative progenitors associated with prominent postnatal growth of the pons. *Nature Communications*, *7*, 11628.
- Lutz, S. E., Zhao, Y., Gulino, M., Lee, S. C., Raine, C. S., & Brosnan, C. F. (2009). Deletion of astrocyte connexins 43 and 30 leads to a dysmyelinating phenotype and hippocampal CA1 vacuolation. *Journal of Neuroscience*, *29*, 7743–7752.
- Marques, S., Zeisel, A., Codeluppi, S., van Bruggen, D., Mendanha Falcao, A., Xiao, L., ... Castelo-Branco G. (2016). Oligodendrocyte heterogeneity in the mouse juvenile and adult central nervous system. *Science*, *352*, 1326–1329.
- Martin, R. J. (2004). Central pontine and extrapontine myelinolysis: The osmotic demyelination syndromes. *The Journal of Neurology, Neurosurgery, and Psychiatry*, *75*(Suppl 3), iii22–iii28.
- Mei, F., Lehmann-Horn, K., Shen, Y. A., Rankin, K. A., Stebbins, K. J., Lorraine, D. S., ... Chan J. R. (2016). Accelerated remyelination during inflammatory demyelination prevents axonal loss and improves functional recovery. *Elife*, *5*.
- Nicaise, C., Mitrecic, D., Demetter, P., De Decker, R., Authalet, M., Boom, A., & Pochet, R. (2009). Impaired blood–brain and blood–spinal cord barriers in mutant SOD1-linked ALS rat. *Brain Research*, *1301*, 152–162.
- Nicaise, C., Putatunda, R., Hala, T. J., Regan, K. A., Frank, D. M., Brion, J. P., ... Lepore, A. C. (2012). Degeneration of phrenic motor neurons induces long-term diaphragm deficits following mid-cervical spinal contusion in mice. *Journal of Neurotrauma*, *29*, 2748–2760.
- Odermatt, B., Wellershaus, K., Wallraff, A., Seifert, G., Degen, J., Euwens, C., ... Steinhäuser, C. and others. (2003). Connexin 47 (Cx47)-deficient mice with enhanced green fluorescent protein reporter gene reveal predominant oligodendrocytic expression of Cx47 and display vacuolized myelin in the CNS. *Journal of Neuroscience*, *23*, 4549–4559.
- Popescu, B. F., Bunyan, R. F., Guo, Y., Parisi, J. E., Lennon, V. A., & Lucchinetti, C. F. (2013). Evidence of aquaporin involvement in human central pontine myelinolysis. *Acta Neuropathologica Communications*, *1*, 40.
- Rojiani, A. M., Cho, E. S., Sharer, L., & Prineas, J. W. (1994). Electrolyte-induced demyelination in rats. 2. Ultrastructural evolution. *Acta Neuropathology*, *88*, 293–299.
- Rose, C. R., & Verkhratsky, A. (2016). Principles of sodium homeostasis and sodium signalling in astroglia. *Glia*, *64*, 1611–1627.
- Sanchez-Guajardo, V., Febbraro, F., Kirik, D., & Romero-Ramos, M. (2010). Microglia acquire distinct activation profiles depending on the degree of  $\alpha$ -synuclein neuropathology in a rAAV based model of Parkinson's disease. *PLoS One*, *5*, e8784.
- Soupart, A., Stenuit, A., Perier, O., & Decaux, G. (1991). Limits of brain tolerance to daily increments in serum sodium in chronically hyponatraemic rats treated with hypertonic saline or urea: Advantages of urea. *Clinical Science (London)*, *80*, 77–84.
- Spasovski, G., Vanholder, R., Allolio, B., Annane, D., Ball, S., Bichet, D., Decaux, G., Fenske, W., ... Hyponatraemia Guideline Development Group. (2014). Clinical practice guideline on diagnosis and treatment of hyponatraemia. *European Journal of Endocrinology*, *170*, G1–47.
- Su, Z., Yuan, Y., Chen, J., Zhu, Y., Qiu, Y., Zhu, F., ... He, C. (2011). Reactive astrocytes inhibit the survival and differentiation of oligodendrocyte precursor cells by secreted TNF- $\alpha$ . *Journal of Neurotrauma*, *28*, 1089–1100.



- Sugimura, Y., Murase, T., Takefuji, S., Hayasaka, S., Takagishi, Y., Oiso, Y., & Murata, Y. (2005). Protective effect of dexamethasone on osmotic-induced demyelination in rats. *Experimental Neurology*, *192*, 178–183.
- Sugimura, Y., Takagi, H., Murase, T., Hoshino, S., Hayasaka, S., Oiso, Y., & Murata, Y. (2002). Prevention of demyelination induced by rapid correction of hyponatremia in mice. *Environmental Medicine*, *46*(1), 2:58–61.
- Suzuki, H., Sugimura, Y., Iwama, S., Suzuki, H., Nobuaki, O., Nagasaki, H., ... Oiso, Y. (2010). Minocycline prevents osmotic demyelination syndrome by inhibiting the activation of microglia. *The Journal of the American Society of Nephrology*, *21*, 2090–2098.
- Takagi, H., Sugimura, Y., Suzuki, H., Iwama, S., Izumida, H., Fujisawa, H., ... Oiso, Y. (2014). Minocycline prevents osmotic demyelination associated with aquaresis. *Kidney International*, *86*, 954–964.
- Takefuji, S., Murase, T., Sugimura, Y., Takagishi, Y., Hayasaka, S., Oiso, Y., & Murata, Y. (2007). Role of microglia in the pathogenesis of osmotic-induced demyelination. *Experimental Neurology*, *204*, 88–94.
- Thurston, J. H., & Hauhart, R. E. (1987). Brain amino acids decrease in chronic hyponatremia and rapid correction causes brain dehydration: Possible clinical significance. *Life Science*, *40*, 2539–2542.
- Thurston, J. H., Hauhart, R. E., & Nelson, J. S. (1987). Adaptive decreases in amino acids (taurine in particular), creatine, and electrolytes prevent cerebral edema in chronically hyponatremic mice: Rapid correction (experimental model of central pontine myelinolysis) causes dehydration and shrinkage of brain. *Metabolic Brain Disease*, *2*, 223–241.
- Tomlinson, B. E., Pierides, A. M., & Bradley, W. G. (1976). Central pontine myelinolysis. Two cases with associated electrolyte disturbance. *QJM: An International Journal of Medicine*, *45*, 373–386.
- Tress, O., Maglione, M., May, D., Pivneva, T., Richter, N., Seyfarth, J., ... Willecke, K. (2012). Panglial gap junctional communication is essential for maintenance of myelin in the CNS. *Journal of Neuroscience*, *32*, 7499–7518.
- Vanden Berghe, T., Linkermann, A., Jouan-Lanhouet, S., Walczak, H., & Vandennebelee, P. (2014). Regulated necrosis: The expanding network of non-apoptotic cell death pathways. *Nature Reviews Molecular Cell Biology*, *15*, 135–147.
- Verbalis, J. G., & Drutarosky, M. D. (1988). Adaptation to chronic hyposmolality in rats. *Kidney International*, *34*, 351–360.
- Woodruff, R. H., & Franklin, R. J. (1999). The expression of myelin protein mRNAs during remyelination of lysolecithin-induced demyelination. *Neuropathology and Applied Neurobiology*, *25*, 226–235.
- Yoon, S., Bogdanov, K., Kovalenko, A., & Wallach, D. (2016). Necroptosis is preceded by nuclear translocation of the signaling proteins that induce it. *Cell Death & Differentiation*, *23*, 253–260.

#### SUPPORTING INFORMATION

Additional Supporting Information may be found online in the supporting information tab for this article.

**How to cite this article:** Bouchat J, Couturier B, Marneffe C, et al. Regional oligodendrocytopathy and astrocytopathy precede myelin loss and blood–brain barrier disruption in a murine model of osmotic demyelination syndrome. *Glia*. 2018;66:606–622. <https://doi.org/10.1002/glia.23268>